Article

Inside Powders: A Theoretical Model of Interfaces between MgO Nanocrystallites

Keith P. McKenna, Peter V. Sushko, and Alexander L. Shluger

J. Am. Chem. Soc., **2007**, 129 (27), 8600-8608• DOI: 10.1021/ja071602m • Publication Date (Web): 15 June 2007

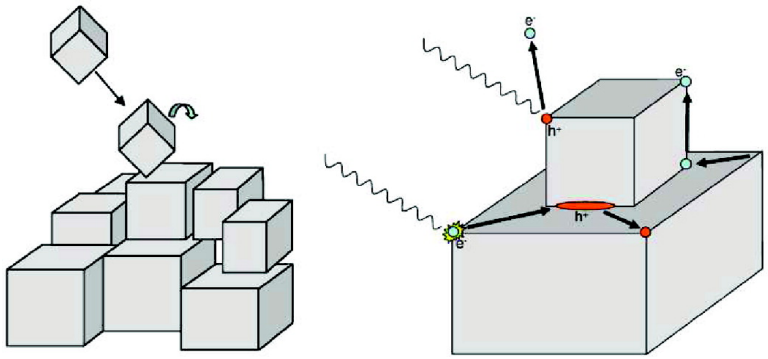

J|A|C|S
ARTICLES
Published on Web 06/15/2007

Inside Powders: A Theoretical Model of Interfaces between MgO Nanocrystallites

Keith P. McKenna,* Peter V. Sushko, and Alexander L. Shluger

Contribution from the Department of Physics and Astronomy, University College London, Gower Street, London WC1E 6BT, U.K., and London Centre for Nanotechnology, 17-19 Gordon Street, London WC1H 0AH, U.K.

Received March 7, 2007; E-mail: k.mckenna@ucl.ac.uk

Abstract: The electron- and hole-trapping and optical properties of a wide variety of interfaces between MgO nanocrystallites are investigated for the first time using a quantum-mechanical embedded-cluster method and time-dependent density functional theory. We conclude that delocalized holes can be transiently trapped at a large number of places within a powder. However, it is more energetically favorable for holes to trap on low-coordinated anions on the nanocrystallite surface, forming O^- species. Electrons are trapped at few interfaces but are readily trapped by surface kink and corner sites. Contrary to common perception, our calculations of optical absorption spectra indicate that a variety of features buried within a powder can be exited with photon energies less than 5 eV, usually used to selectively excite low-coordinated surface sites.

1. Introduction

Nanocrystalline ceramic materials with crystallites of 1−10 nm in dimension form a new class of materials with unique hybrid properties characteristic of neither the molecular nor the bulk solid-state limits. The large number of atoms located at the edges and on the surfaces of individual nanocrystallites provide active sites for surface reactions.[1,2] Most of the samples used in practical applications are powders with ultrahigh surface-to-volume ratio.[3−7] Their enhanced chemical activity is often associated with electron- and hole-trapping and the formation of O^- species at nanocrystallite surfaces.[8,9] Surprisingly little is known, however, about the electron- and hole-trapping at contacts and interfaces between nanocrystallites. In this paper we use theoretical modeling to develop a more balanced view of the mechanisms of charging and chemical activation of nanopowders by considering both low-coordinated surface features and interfaces between nanocrystallites inside the powder.

The trapping of electrons and holes in insulating oxide materials, which can be both very useful and harmful, is an important issue of wider interest. Electrons and holes can be produced thermally, mechanically, electrically, and by irradiation with particles or photons. Commonly used experimental probes such as X-ray and UV photoelectron spectroscopy and transmission electron microscopy (TEM), for example, may cause charge to be trapped in the material (often powder) directly or as a consequence of secondary processes. Although the Coulomb interaction favors the recombination of electrons and holes, they may become separated and trapped in configurations which are thermally stable over long time scales. It has long been known that charge can be localized near defects in the bulk of an insulator, such as vacancies.[10,11] However, charge can also be trapped at topological features on surfaces, such as steps and kinks.[12,13] Surface sites which possess trapped charge are often associated with high chemical reactivity; therefore, they have important applications for catalysis.[8,9]

Charge-trapping can also occur at interfaces between different materials and at grain boundaries. This is a critical issue for technologically important electronic devices, such as magnetic tunnel junctions[14] and CMOS transistors,[15] and optical devices, such as nanostructured light-emitting diodes. In these systems, electrons and holes can be injected electrically, and charge-trapping may adversely affect the device performance. Charge-trapping at interfaces also has important applications to the understanding of tribocharging.[16] It has been suggested that electron and hole formation and subsequent trapping may be

(1) Nieves, I.; Klabunde, K. J. *Mater. Chem.* **1988**, *18*, 485.
(2) Itoh, H.; Utampanya, S.; Stark, J. V.; Klabunde, K. J.; Schulp, J. R. *Chem. Mater.* **1993**, *5*, 71.
(3) Becker, A.; Benfer, S.; Hofmann, P.; Jacob, K.-H.; Knözinger, E. *Ber. Bunsenges. Phys. Chem.* **1995**, *99*, 1328.
(4) Giamello, E.; Paganini, M. C.; Murphy, D. M.; Ferrari, A. M.; Pacchioni, G. *J. Phys. Chem. B* **1997**, *101*, 971−982.
(5) Hackley, V. A.; Stoimenov, P. K.; Ho, D. L.; Sung, L. P.; Klabunde, K. J. *J. Appl. Crystallogr.* **2005**, *38*, 619.
(6) Knözinger, E.; Diwald, O.; Sterrer, M. *J. Mol. Catal. A* **2000**, *162*, 83.
(7) Stankic, S.; Müller, M.; Diwald, O.; Sterrer, M.; Knözinger, E.; Bernardi, J. *Angew. Chem., Int. Ed* **2005**, *44*, 4917.
(8) Zecchina, A.; Scarano, D.; Bordiga, S.; Spoto, G.; Lamberti, C. *Adv. Catal.* **2001**, *46*, 265.
(9) Spoto, G.; Gribov, E.; Ricchiardi, G.; Damin, A.; Scarano, D.; Bordiga, S.; Lamberti, C.; Zecchina, A. *Prog. Surf. Sci.* **2004**, *71*, 76.
(10) de Boer, J. H. *Recl. Trav. Chim. Pays-Bas* **1937**, *56*, 301.
(11) Feher, G. *Phys. Rev.* **1957**, *105*, 1122.
(12) Sushko, P. V.; Gavartin, J. L.; Shluger, A. L. *J. Phys. Chem. B* **2002**, *106*, 2269−2276.
(13) Chiesa, M.; Paganini, M. C.; Giamello, E.; Valentin, C. D.; Pacchioni, G. *Angew. Chem., Int. Ed.* **2003**, *42*, 1759−1761.
(14) Gokcea, A.; Nowak, E. R.; Yang, S. H.; Parkin, S. S. P. *J. Appl. Phys.* **2006**, *99*, 08A906.
(15) Houssa, M.; Stesmans, A.; Naili, M.; Heyns, M. M. *Appl. Phys. Lett.* **2000**, *77*, 1381−1383.
(16) Stoneham, A. M. *IEEE Trans. Dielectr. Electr. Insul.* **1997**, *4*, 604−613.

10.1021/ja071602m CCC: $37.00

responsible for the dramatic electrostatic and optical phenomena that are observed during seismic activity.[17] In the other extreme of pressure, oxide nanoparticles are abundant in interstellar dust,[18−20] and charge buildup in insulating materials has important implications for space exploration.[21]

MgO is one of the ideal systems for studying these diverse phenomena because its physical and chemical properties are well characterized and because highly uniform powders can be produced with essentially only (100) surface exposure.[3,6] Charge-trapping in MgO has continued to receive a great deal of interest, both theoretically and experimentally. Topological features on the surface of thin films of MgO and defects in various charge states have recently been studied using scanning tunneling spectroscopy and electron paramagnetic resonance (EPR) spectroscopy.[22−25] High-surface-area MgO nanopowders have been produced using chemical vapor deposition with uniform and controllable sizes of nanocrystallites.[3,6] These advances facilitated the application of optical techniques such as UV−vis spectroscopy and photoluminescence to probe the properties of low-coordinated features, such as steps, corners, and kinks.[7] Many theoretical works have investigated the optical, electronic, and chemical properties of various features found on the surface of MgO nanocrystallites.[4,12,13,26−30] It has been demonstrated that photons of energy less than about 5 eV can excite selectively low-coordinated sites. These sites are usually assumed to be located at surfaces, but no data exist regarding the optical absorption spectra of more complex features, such as contact sites and interfaces between nanocrystallites. A large number of interfaces with different structures are present in powders (see, for example, TEM images in refs 30−32), and in some cases resemble interfaces that can be found in polycrystalline films. EPR studies of MgO nanopowders that were exposed to photons of different energy indicate that a significant number of electrons and holes can be trapped at places in the powder, and the mechanisms of their formation have recently been investigated.[33] Some of the holes are, however, thought to be EPR-invisible.[34] It was suggested that these holes may be delocalized at interfaces between nanocrystallites. However, to date there have been no calculations to confirm this conjecture.

In this paper we address important and quite general issues of optical absorption and electron- and hole-trapping at interfaces between nanocrystallites by using a quantum-mechanical embedded-cluster method. These issues are also relevant for similar materials such as NiO and CoO, which have the same lattice structure, as well as for other oxides, such as TiO_2, ZrO_2, and CeO_2.

To summarize the main results: A broad survey of possible features that can be found in MgO nanopowders has been conducted. Electron-trapping is found to be strongest on surface features of nanocrystallites such as cation-terminated step corners and free corners. A very shallow electron trap is also found at one of the interfaces between nanocrystallites that has been considered. The trapping of localized holes at interfaces between nanocrystallites is shown to be quite unlikely—the only candidate sites occurring at constrained interfaces between nanocrystallites, which may be present in very small concentrations. Delocalized holes can be readily trapped at interfaces; however, they need only overcome a small barrier, of the order 0.4 eV, to escape onto terraces and edges and reach more favorable sites from there. Calculations of the optical properties of MgO nanopowders, using time-dependent density functional theory[35−37] (TD-DFT), indicate that a range of features both on the surface and inside the powder may be excited by photons with energies below 5 eV. The combination of these results allows one to suggest ways in which excitons can be formed and the places to which the electrons and holes may subsequently migrate.

The paper is organized in the following way. In section 2, the types of interfaces that may be found in an MgO nanopowder are discussed, and those features for which we will calculate charge-trapping and optical excitation spectra are identified. The embedded-cluster method that is used for this investigation is described in section 3, together with details of the implementation for interfaces between nanocrystallites. In section 4, results are presented for the geometry of interfaces, their local electronic structure, electron- and hole-trapping, and optical absorption. Finally, the main results and our conclusions are presented.

2. Models of Interfaces between MgO Nanocrystallites

The morphology of MgO nanocrystallites in powders depends upon the method and conditions used for their fabrication. For example, large MgO cubes ($L \sim 50$ nm) can be produced as smoke particles by burning magnesium in air. MgO nanocrystallites, with a 1−5 nm scale diameter, have been produced using chemical vapor deposition[3,6,7] (CVD) with a high degree of size selectivity. Exotic nanoflower structures have been fabricated in kinetically driven growth conditions.[38] MgO nanocrystallites can also be produced by chemical decomposition of magnesium hydroxide[4] and sol−gel techniques.[5] Powders of cubic MgO nanocrystallites can be obtained by collecting the nanocrystallites, formed in a CVD chamber, for example, onto a support. As nanocrystallites land on the growing pile (see Figure 1a),

(17) Takeuchi, A.; Nagahamab, H.; Hashimotoa, T. *Phys. Chem. Earth, Parts A/B/C* **2004**, *29*, 359−366.
(18) Duley, W. W. *Astrophys. Space Sci.* **1982**, *88*, 501.
(19) Koehler, T. M.; Gail, H.-P.; Sedlmayr, E. *Astron. Astrophys.* **1997**, *320*, 553.
(20) Ferrarotti, A. S.; Gail, H.-P. *Astron. Astrophys.* **2001**, *371*, 133.
(21) Gross, F. B. *J. Electrostat.* **2003**, *58*, 147−156.
(22) Sterrer, M.; Fischbach, E.; Risse, T.; Freund, H.-J. *Phys. Rev. Lett.* **2005**, *94*, 186101.
(23) Chiesa, M.; Giamello, E.; Valentin, C. D.; Pacchioni, G. *Chem. Phys. Lett.* **2005**, *403*, 124.
(24) Sterrer, M.; Heyde, M.; Novicki, M.; Nilius, N.; Risse, T.; Rust, H.-P.; Pacchioni, G.; Freund, H.-J. *J. Phys. Chem. B* **2006**, *110*, 46.
(25) Sterrer, M.; Fischbach, E.; Heyde, M.; Nilius, N.; Rust, H.-P.; Risse, T.; Freund, H.-J. *J. Phys. Chem. B* **2006**, *110*, 8665.
(26) Shluger, A. L.; Catlow, C. R. A.; Grimes, R. W.; Itoh, N. *J. Phys.: Condens. Matter* **1991**, *3*, 8027.
(27) Shluger, A. L.; Sushko, P. V.; Kantorovich, L. N. *Phys. Rev. B* **1999**, *59*, 2417−2430.
(28) Sushko, P. V.; Shluger, A. L.; Catlow, C. R. A. *Surf. Sci.* **2000**, *450*, 153−170.
(29) Ricci, D.; Pacchioni, G.; Sushko, P. V.; Shluger, A. L. *J. Chem. Phys.* **2002**, *117*, 18444.
(30) Chiesa, M.; Paganini, M. C.; Spoto, G.; Giamello, E.; Valentin, C. D.; Vitto, A. D.; Pacchioni, G. *J. Phys. Chem. B* **2005**, *109*, 7314.
(31) Berger, T.; Sterrer, M.; Stankic, S.; Bernardi, J.; Diwald, O.; Knözinger, E. *Mater. Sci. Eng. C* **2005**, *25*, 664−668.
(32) Stankic, S.; Bernardi, J.; Diwald, O.; Knözinger, E. *J. Phys. Chem. B* **2006**, *110*, 13866−13871.
(33) Trevisanutto, P. E.; Sushko, P. V.; Shluger, A. L.; Beck, K. M.; Henyk, M.; Joly, A. G.; Hess, W. P. *Surf. Sci.* **2005**, *593*, 210−220.
(34) Sterrer, M.; Diwald, O.; Knözinger, E.; Sushko, P. V.; Shluger, A. L. *J. Phys. Chem. B* **2002**, *106*, 12478−12482.
(35) Bauernschmitt, R.; Ahlrichs, R. *Chem. Phys. Lett.* **1996**, *256*, 454.
(36) Casida, M. E.; Jamorski, C.; Casida, K. C.; Salahub, D. R. *J. Chem. Phys.* **1998**, *108*, 4439.
(37) Stratmann, R. E.; Scuseria, G. E.; Frisch, M. J. *J. Chem. Phys.* **1998**, *109*, 8218.
(38) Hao, Y.; Meng, G.; Ye, C.; Zhang, X.; Zhang, L. *J. Phys. Chem. B* **2005**, *109*, 11204.

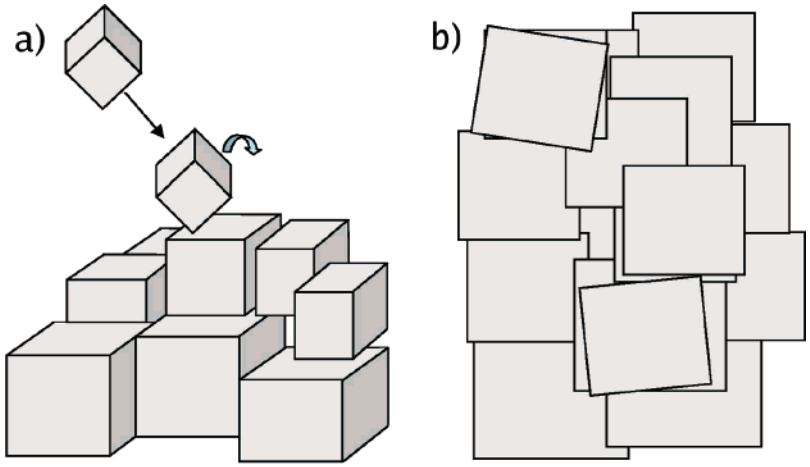

Figure 1. (a) MgO nanocrystallites, formed in a CVD chamber, for example, are swept into the growing pile by convection currents. Following contact with the pile, they may rotate and translate with respect to other nanocrystallites before resting in a configuration corresponding to a local minimum of the potential energy. (b) A powder produced in this way consists mainly of interfaces between (100) terraces, as shown by TEM studies.[30,32,39]

they may rotate and translate with respect to other nanocrystallites before finding a configuration corresponding to a local minimum in the potential energy.

A powder produced in this way may have high densities of different types of topological feature, including low-coordinated corners, edges, and steps on the surfaces of nanocrystallites and interfaces between the (100) terraces of two different nanocrystallites, which are rotated with respect to each other. Transmission electron microscopy studies of MgO smoke particles have revealed a preference for alignment of nanocrystallites with commensurate (100) surfaces. However, a small number of nanocrystallites were found to be misaligned at angles corresponding to high-site-coincidence (100) twist grain boundaries[39] (see Figure 1b). In addition, one may also find very metastable interfaces between nanocrystallites, which exist as a consequence of geometrical constraints imposed by surrounding nanocrystallites. If the powder is subjected to high-temperature annealing after collection, a degree of sintering may occur, and most of the metastable configurations should transform into lower energy configurations. Experimentally, CVD powders are pressed into pellets before IR studies can be performed. We note that surfaces of annealed samples are usually dehydroxylated, and in this paper we neglect the presence of water in the samples.

A number of local structural features that can be found at interfaces between nanocrystallites within a powder have been selected for investigation. Figure 2 shows the geometry of each of these on the nanometer scale and highlights the local region that is considered for charge-trapping and optical absorption. While these configurations are not exhaustive, they do account for the most probable structures that are found in nanopowders. For completeness, a number of features on the surface of nanocrystallites, and also interfaces between nanocrystallites which are geometrically constrained, are included. The structures that are studied can be divided into three broad categories and are described in more detail below.

(I) Nanocrystallite Surface. Type I features are found on the outer surface of individual nanocrystallites. From this category we consider the edge (E), terrace (T), anion- and cation-terminated corners (denoted O-C and Mg-C, respectively), and

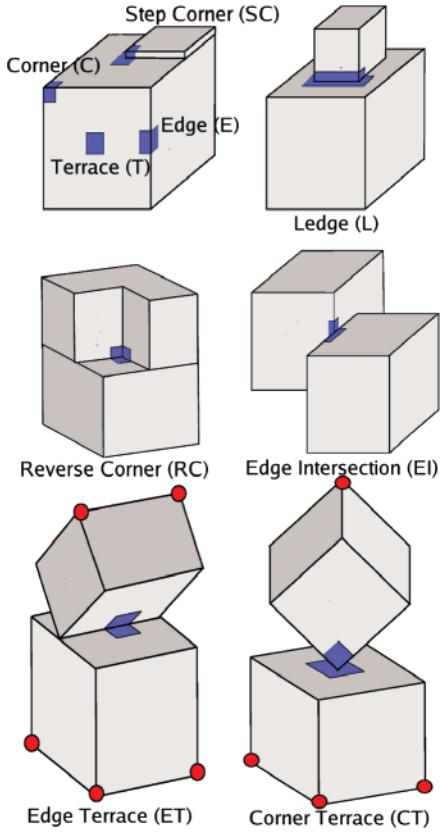

Figure 2. Features on the surface of MgO nanocrystallites and at interfaces between them that we have considered for our calculations. More detailed descriptions can be found in the text.

anion- and cation-terminated step-corners (O-SC and Mg-SC, respectively), as indicated in Figure 2. A number of other surface features have been considered in previous work—for example, the step and step-kink.[12]

(II) Nanocrystallite Interfaces I. Type II features occur at the interface between two nanocrystallites which contact by commensurate (100) facets (see Figure 1b). These structures are not, strictly speaking, interfaces at all, as the lattices have full site coincidence. However, each nanocrystallite has the Wulff morphology expected for an isolated nanocrystallite, and there is also a distribution of sizes; therefore, the classification of these structures as interfaces is useful. One of the features

(39) Chaudhari, P.; Matthews, J. W. *J. Appl. Phys.* **1971**, *42*, 3063.

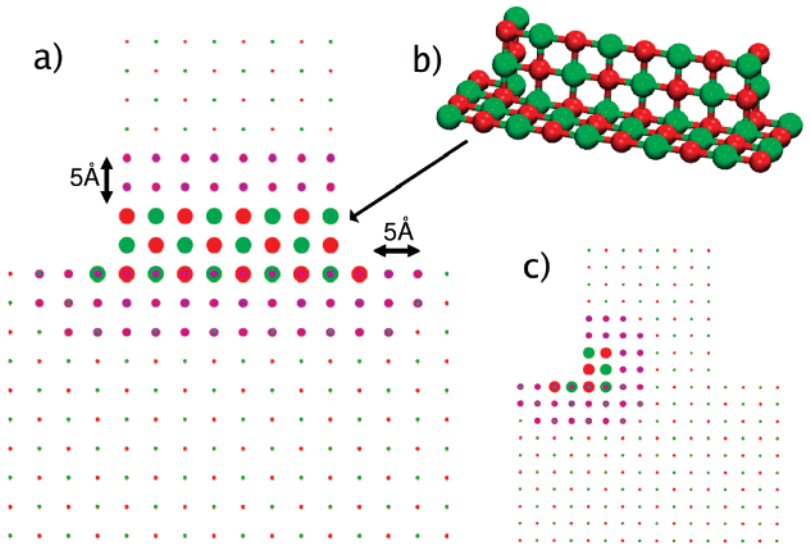

Figure 3. Illustration of the embedded-cluster model for the ledge feature, labeled L in Figure 2. Front (a) and side (c) views of the system are shown. The region of interest is the interface between the cubes along one of the edges. The quantum cluster (b) contains 54 ions, indicated in the figure by large points. A total of 153 interface Mg ions surround the quantum cluster, indicated by medium-sized points. The remaining ions, indicated by small points, are treated classically.

of this type is referred to as a ledge (L). The local region of interest runs along the (001) direction, as indicated in Figure 2. A ledge which contains 8 MgO molecules along its length is selected for this study, therefore terminating in an anion at one edge and a cation at the opposite end. A feature we denote as an reverse corner (RC) is also included in this category. It can be centered on either an anion or a cation, and both possibilities are investigated (referred to as O-RC and Mg-RC, respectively). Finally, the region of intersection between two edges of two different MgO cubes, referred to as an edge intersection (EI), is considered.

(III) Nanocrystallite Interfaces II. Type III features are interfaces between two separate nanocrystallites which are not of type II; therefore, they are generally of higher energy. Such interfaces may be formed as surrounding nanocrystallites within the powder may prevent the re-orientation required to reach a lower energy configuration. These types of interface may be prolific in powders that are not annealed and in pellets that have been pressed. The number of possible interfaces of this kind is large, as a distribution of local constraints may produce interfaces with different properties. In this study, only two simple and quite symmetric types of interface are selected to indicate the type of effects one may find there. These consist of an edge resting upon a terrace, denoted as an edge-terrace (ET) feature, and a corner resting upon a terrace, denoted as a corner-terrace (CT) feature (Figure 2). The corner that contacts the terrace may be terminated by an anion or a cation. Both possibilities are considered and referred to as O-CT and Mg-CT, respectively. These local features, besides existing as possible metastable configurations, resemble local structures which may be found in tilt and twist grain boundaries.

To construct the constrained interfaces described above, we initially optimize the geometry of an isolated nanocube containing 1000 ions in a $10 \times 10 \times 10$ structure. Two of these cubes are then oriented with respect to each other and aligned so their lattices are commensurate at the point of contact. The total energy of the combined system is then minimized; however, a number of ions are held fixed to enforce the constraints that are imposed by the surrounding nanocrystallites (these are indicated in Figure 2 by filled circles).

3. Embedded-Cluster Method

Topological features on MgO nanocrystallites and interfaces between them are modeled using an embedded-cluster method. This technique consistently combines quantum-mechanical and classical methods to enable large systems to be studied and to ensure accurate description of long-range polarization effects. Classical ions are described using empirical pair potentials, and quantum-mechanical ions are treated using hybrid density functional theory and Gaussian basis sets. This method is implemented in the GUESS code.[12,28,40]

The majority of the ions that make up the nanocrystallite (which may number in the thousands) are modeled using the empirical polarizable shell model potential of Lewis and Catlow.[41] Ions that are close to the feature of interest (highlighted in Figure 2) are described quantum-mechanically by interfacing to the Gaussian03[42] code. Figure 3 shows the setup for the ledge feature (Figure 2), where 54 atoms are treated at an all-electron quantum level and form the quantum cluster. The B3LYP hybrid density functional is used, which combines Becke's hybrid exchange functional[43] with the correlation functional of Lee, Yang, and Parr.[44] The amount of exact exchange that is used can affect the degree of electron and hole localization.[45−47] The parametrization that we have used has been previously applied to calculate a wide range of MgO properties. The results, which include the optical excitation energies of low-coordinated surface sites,[12,28] EPR properties of electrons and holes trapped at various defect sites,[30,48,49] and photo-

(40) Sushko, P. V.; Shluger, A. L.; Baetzold, R. C.; Catlow, C. R. A. *J. Phys: Condens. Matter* **2000**, *12*, 8257.
(41) Lewis, G. V.; Catlow, C. R. A. *J. Phys. C: Solid State Phys.* **2004**, *18*, 1149.
(42) Frisch, M. J.; et al. *Gaussian 03*, Revision C.02; Gaussian, Inc.: Wallingford, CT, 2004.
(43) Becke, A. D. *J. Chem. Phys.* **1993**, *98*, 5648.
(44) Lee, C.; Yang, W.; Parr, R. G. *Phys. Rev. B* **1988**, *37*, 785.
(45) Lægsgaard, J.; Stokbro, K. *Phys. Rev. Lett.* **2001**, *86*, 2834−2837.
(46) Pacchioni, G.; Frigoli, F.; Ricci, D.; Weil, J. A. *Phys. Rev. B* **2000**, *63*, 054102.
(47) Gavartin, J. L.; Sushko, P. V.; Shluger, A. L. *Phys. Rev. B* **2003**, *67*, 035108.
(48) Ojamae, L.; Pisani, C. *J. Chem. Phys.* **1998**, *109*, 10984.
(49) Chiesa, M.; Paganini, M. C.; Giamello, E.; Murphy, D. M.; Valentin, C. D.; Pacchioni, G. *Acc. Chem. Res.* **2006**, *39*, 861−867.

Table 1. Composition of the Quantum Cluster Including Interface Mg Ions, Together with the Characteristic Dimensions of the Nanocrystallite(s), for Each Feature Considered Using the Embedded Cluster Method

feature	composition of quantum cluster	characteristic dimensions of the system
Mg-C	$Mg_{14}O_{13}Mg^*_4$	$2 \times 2 \times 2$ nm
O-C	$Mg_{13}O_{14}Mg^*_{43}$	$2 \times 2 \times 2$ nm
T	$Mg_{14}O_{13}Mg^*_{89}$	$2 \times 2 \times 2$ nm
E	$Mg_{14}O_{13}Mg^*_{62}$	$2 \times 2 \times 2$ nm
O-SC	$Mg_{11}O_{11}Mg^*_{24}$	$5 \times 5 \times 5$ nm
Mg-SC	$Mg_{11}O_{11}Mg^*_{24}$	$5 \times 5 \times 5$ nm
L	$Mg_{27}O_{27}Mg^*_{153}$	$3 \times 3 \times 3$ nm + $1.5 \times 1.5 \times 1.5$ nm
O-RC	$Mg_{28}O_{28}Mg^*_{150}$	$3 \times 3 \times 3$ nm
Mg-RC	$Mg_{28}O_{28}Mg^*_{150}$	$3 \times 3 \times 3$ nm
EI	$Mg_{24}O_{24}Mg^*_{104}$	$2 \times 2 \times 2$ nm + $2 \times 2 \times 2$ nm
ET	$Mg_{15}O_{15}Mg^*_{105}$	$2 \times 2 \times 2$ nm + $2 \times 2 \times 2$ nm
O-CT	$Mg_{23}O_{22}Mg^*_{100}$	$2 \times 2 \times 2$ nm + $2 \times 2 \times 2$ nm
Mg-CT	$Mg_{22}O_{23}Mg^*_{100}$	$2 \times 2 \times 2$ nm + $2 \times 2 \times 2$ nm

stimulated desorption,[33,50] are in good agreement with experiments. This gives us confidence that this scheme can accurately account for the balance of energetics concerning electron- and hole-trapping in MgO. As in previous studies,[12,28] we used the standard Gaussian 6-31G basis set. However, in the case of calculations of electron affinity, the basis set is extended to 6-311G and 6-311+G to ensure the convergence. In order to prevent spurious spilling of the wavefunction from the quantum cluster into the classically modeled regions, first and second nearest-neighbor Mg ions are substituted for interface Mg ions (denoted as Mg*), as shown in Figure 3. Interface Mg ions are modeled using a semi-local effective core pseudopotential possessing no associated basis functions.

The total energy of the quantum cluster, in the presence of the electrostatic potential produced by all surrounding classical ions, is calculated by solving the Kohn−Sham equations. The forces acting on all ions are then calculated, and the geometry of the entire system is optimized self-consistently using the BFGS algorithm.

In total, six surface features and seven interfaces have been identified for investigation. Table 1 summarizes the composition of the quantum cluster and the dimensions of the system for each of them. The corner, edge, and terrace features are each modeled with a $3 \times 3 \times 3$ ions quantum cluster. The edge cluster is centered on an O ion, and the terrace is centered on a Mg ion. The corner-terrace and edge-terrace features are modeled with clusters formed by combining the quantum clusters of the isolated corner, edge, and terrace (Figure 2). The quantum cluster for the step-corner includes 8 ions which are near the corner on the upper part of the step and 16 ions which are below it in a 4×4 configuration (see Figure 6).

4. Results and Discussion

4.1. Structure Relaxation. The geometry of each feature described in the previous section was initially optimized using classical potentials and then self-consistently relaxed using the embedded-cluster model. The total energy of the quantum cluster was converged to 3×10^{-9} eV, and forces were minimized to a tolerance of 1.9×10^{-5} eV Å^{-1}. The lowest energy structure of surface and interface features is modified compared to that of the bulk. For example, the three-coordinated anion and cation at the corner relax inward slightly so that the - nearest-neighbor O−Mg distances are 2.02 and 1.96 Å, respectively. This is compared to an average Mg−O distance in the bulk of 2.15 Å,

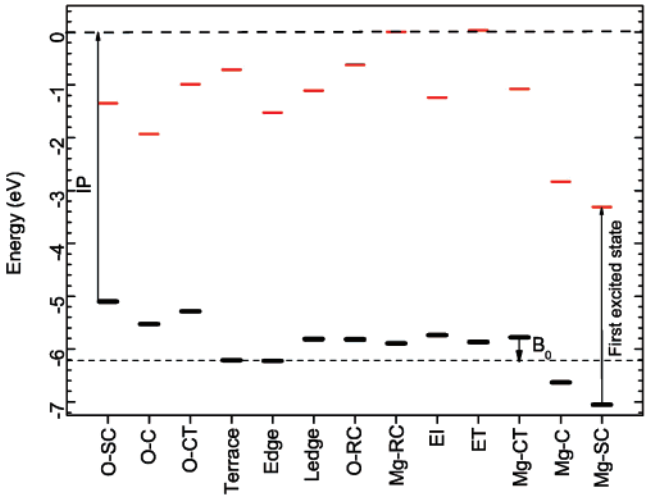

Figure 4. Approximate positions of the highest occupied level (black lines) estimated by calculating IPs and the lowest unoccupied level (red lines) with respect to the vacuum level (0 eV). The dashed line indicates the IP of the edge and terrace. The energy required for holes trapped at interfaces to escape, B_0, is also shown (see section 4.3).

calculated using the embedded-cluster method. Geometrical relaxation is generally weaker for more coordinated interfaces.

For the case of the metastable configurations consisting of a corner or an edge resting upon a terrace, a continuum of possible geometries may be realized in reality because of the variety of constraints that surrounding nanocrystallites may impose. In these calculations, two highly symmetric situations are considered. The cubes are aligned with respect to each other, and a number of atoms in each cube that are far from the interface are held fixed (filled circles in Figure 2). The initial distance between the fixed points, before the structure is relaxed, can be varied corresponding to a range of local strains. However, the local geometry of the interface is only weakly dependent on the total strain, as this is distributed over a large region surrounding the interface. For the Mg corner in contact with an O atom of the terrace, the relaxed interfacial Mg−O distance is 1.93 Å, while for the O corner on the terrace it is 1.88 Å. The geometry of the edge-terrace interface is relatively unperturbed from the geometry of its constituent parts separately, and the interfacial Mg−O distance is 1.96 Å.

4.2. Local Electronic Structure. The electronic structure of all features in the ground state consists of a filled valence band comprised of O 2p-states and an unoccupied conduction band which has Mg 3s-state nature. The difference between the highest occupied and lowest unoccupied single-electron levels of each feature depends upon the local ion coordination, ranging from 6.2 eV for the ideal terrace to 4.4 eV at the anion corner. Examining the local electronic structure of each topological feature can help interpret where electrons or holes may prefer to reside, and also allows estimation of barriers to their motion. The vacuum level provides a convenient reference point from which to compare the relative positions of electronic levels corresponding to each feature. The vertical ionization potential (IP) defines the position of the highest occupied level with respect to the vacuum, as shown in Figure 4. IPs have been calculated allowing relaxation of the electronic density and the polarization in the classically modeled regions, by optimizing the positions of the shells on O ions (Table 2). In addition, TD-DFT has also been used to calculate the first excited singlet

(50) Hess, W. P.; Joly, A. G.; Beck, K. M.; Henyk, M.; Sushko, P. V.; Trevisanutto, P. E.; Shluger, A. L. *J. Phys. Chem. B* **2005**, *109*, 19563−19578.

Table 2. Vertical Ionization Potentials and Electron Affinities for Each of the Features Considered[a]

feature	IP (eV)	B_0 (eV)	EA_v (eV)	EA_r (eV)
Mg-C	6.63	−0.42	0.03	0.56
O-C	5.53	0.68	−1.23	
T	6.21		−1.39	
E	6.21		−0.94	
O-SC	5.10	1.11	−0.73	
Mg-SC	7.05	−0.84	0.52	1.33
L	5.81	0.40	−0.69	0.07
O-RC	5.82	0.39	−1.27	
Mg-RC	5.89	0.33	−1.30	
EI	5.74	0.47	−0.85	
ET	5.87	0.34	−2.11	
O-CT	5.29	0.92	−1.11	
Mg-CT	5.78	0.43	−0.27	−0.17

[a] IP is the ionization potential, B_0 the approximate barrier for holes to escape onto the terraces and edges of nanocrystallites, EA_v the vertical electron affinity (obtained with the 6-31G basis set), including relaxation of electronic density and polarization of classical ions, and EA_r the fully relaxed electron affinity obtained.

state for each system. To give an indication of position of the lowest unoccupied state for each feature, the IP is used as a reference, and the aligned levels are also shown in Figure 4.

Given that all the quantum clusters are treated at a similar level, the relative alignment of these levels is valid; however, to obtain quantitatively accurate values for the IP, one should converge results with respect to quantum cluster size and basis set in each case. For example, the ideal terrace, which is an example with particularly slow convergence, the IP has been shown in previous studies to approach 6.7 eV.[28] This differs by 0.5 eV from the calculation presented here, and this gives a reasonable upper estimate of the effect of improving the quantum cluster size and basis set.

4.3. Hole Trapping and Localization. Localization of electrons and holes is governed by a balance of energies resulting from electrostatic potential distribution, local geometrical distortion, and polarization of the nanocrystal. The values of vertical IP shown in Figure 4 allow one to compare the relative energy for holes located in different places. The O-SC, O-C, and O-CT are the most favorable of the places we have considered for holes to reside. However, the constrained O-CT interface is expected to have a small concentration in real powders. The spin density is shown on the left of Figure 5 for the O-SC and O-C. When the geometry is allowed to relax, the total energy decreases and the hole becomes more localized on the three-coordinated anion, as shown on the right of Figure 5. The nature of the geometrical distortion, for both the O-SC and the O-C, is relaxation of neighboring Mg ions away from the three-coordinated anion. The decrease in total energy is 0.80 eV for the O-C and 0.87 eV for the O−SC. The only other structural features where the hole is able to localize are the O-CT and Mg-CT features. In these extremely nonequilibrium metastable arrangements of nanocrystallites, the hole is localized over two O ions which belong to different nanocrystallites, forming an O_2^{3-} species.

The remaining features we have considered exhibit only a very small geometrical change following relaxation, and the holes remained delocalized over the oxygen ions at the interface. Although delocalized, these holes can still be trapped at those topological features where energetic barriers prevent their escape. From the data shown in Table 2 and Figure 4, we estimate a lower limit for the barrier to hole motion by

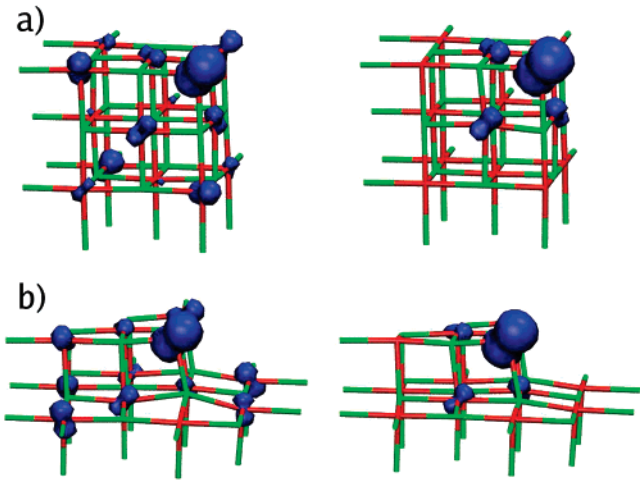

Figure 5. Spin density of the hole at the O corner (a) and O step-corner (b) before (left) and after (right) relaxation of the geometry. Isosurfaces corresponding to 0.05 e $Å^{-3}$ are shown.

comparing the alignment of IPs for each topological feature. To transfer from a metastable to a stable trapping site, a hole should first escape to the edge or the terrace, which provides percolation paths in order for it to move elsewhere. Our calculations indicate that the IPs for both the edge and the terrace lie very close to each other, and this is indicated by the dashed line in Figure 4.

The quantity B_0 is defined as the difference in energy between the vertical IP for a particular feature and that for the edge and terrace. Positive values of B_0 indicate that the hole could be transiently trapped at some feature before escaping to the edge or terrace; i.e., B_0 represents a lower limit for the difference in energy as the effect of geometrical relaxation can only increase it by decreasing the total energy. Table 2 summarizes the IPs for each of the features studied, together with values of B_0 for each feature. For delocalized holes, B_0 is a good approximation to the energy difference, and one can see that holes can be trapped at a variety of interfaces. The typical difference in energy is about 0.4 eV, which should be accessible thermally at room temperature. This picture is consistent with an experimental study which has shown that holes which are optically excited away from low-coordinated corners return to the corners over a characteristic time scale (of the order minutes) after the excitation source is switched off.[34]

4.4. Electron Trapping. The electron affinity has been calculated for a number of the features considered. As not all of the features are able to trap electrons, the following procedure is adopted to minimize the computational cost. First, a "vertical" electron affinity (EA_v) is calculated using the 6-31G basis set. In this calculation all ion positions are fixed, but relaxation of the electronic density and polarization of classical O ions are included. If EA_v, for a given feature, is very negative, then it is unlikely that increasing the size of the basis set and allowing relaxation of ion positions will make it positive. Therefore, we select a number of candidate features with positive or close to zero EA_v, on which to calculate the fully converged electron affinity (EA_r). The lower bound for this restricted subset is chosen as −0.7 eV. The convergence of the electron affinity is then investigated by increasing the basis set from 6-31G to 6-311+G on both Mg and O ions. Values of EA_v and relaxed EA (EA_r) are shown in Table 2.

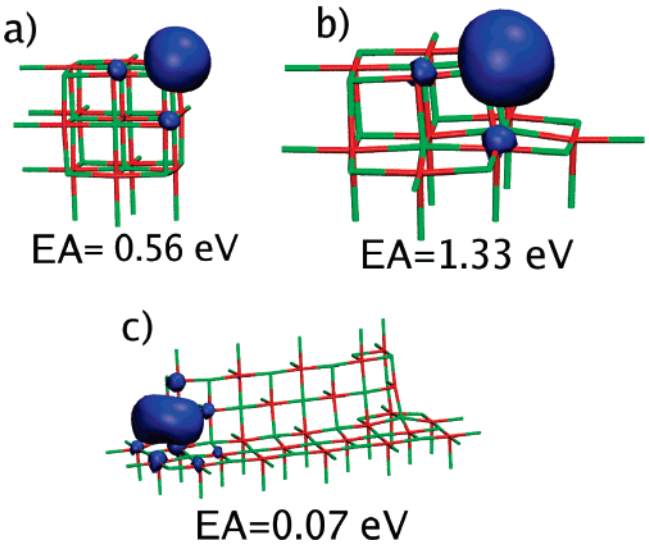

Figure 6. Spin density of the electron at the Mg−C (a), Mg−SC (b), and ledge (c) after full relaxation of the geometry. Isosurfaces corresponding to 0.002 e Å^{-3} are shown.

Only four of the features studied possess EA_v above the −0.7 eV cutoff: the ledge, Mg-C, Mg-SC, and Mg-CT. The Mg-SC has the highest relaxed electron affinity of all the features investigated, 1.33 eV. After electron-trapping, the separation between the three-coordinated Mg ion and the four-coordinated O ions changes from 1.92 to 2.02 Å, and the separation between the three-coordinated Mg ion and the six-coordinated O ion changes from 2.01 to 2.35 Å (Figure 6b). The Mg-C has an electron affinity of 0.56 eV, and associated with the charge-trapping is local relaxation of the neighboring O ions away form the Mg ion: the separation increases from 1.96 to 2.08 Å (Figure 6a). In both of these cases, the electron is well localized on the three-coordinated Mg ion (Figure 6) and produces an occupied level the middle of the MgO band gap.

The ledge is found to be a shallow electron trap, with a very small electron affinity of 0.07 eV. The trapped electron is rather loosely bound to the cation edge of the ledge feature (Figure 6c). The geometrical relaxation involves the outward relaxation of the four-coordinated cation and the depression of the neighboring six-coordinated anion into the surface. For the Mg-CT feature, the electron affinity remains negative after increasing the basis set; therefore, this feature is not a potential electron trap. The physical interpretation of this fact is that the positive affinity of the free cation corner is removed by the presence of the nearby MgO surface in the Mg-CT structure.

Investigating convergence of the electron affinity, we find that the effect of adding more diffuse functions to the O atoms is small, whereas adding diffuse functions on Mg ions increases EA_v by about 0.3 eV. However, for the features which can trap an electron, EA_r is much less affected by the diffuse Mg basis; typical differences are less than 0.1 eV. This is because electrons are well localized in these cases, and this gives us confidence that these values are well converged.

4.5. Optical Absorption. Optical absorption spectra for each of the features in Figure 2 have been calculated using TD-DFT. The 10 lowest singlet−singlet transitions have been calculated. The energies of the strongest excitation peaks, their oscillator strength, and a description of the electronic transitions involved are summarized in Table 3. Providing that the initial and final states involved in the electronic transition are localized within the quantum cluster, the calculated excitation energies should not depend on the size and shape of the quantum cluster used for embedding.

Table 3. Optical Excitation of Various Local Features in an MgO Powder[a]

feature	*E*	*f*	description of transition
Mg-C	4.25	0.11	6C O to 3C Mg
O-C	4.66	0.12	6C O to 4C Mg
terrace[b]	5.78	0.17	5C O to 5C surface
edge[b]	4.6−5.5		
O-SC	4.79	0.08	4C/5C O to 4C/5C O
Mg-SC	4.08	0.04	4C O to 3C Mg
ledge	4.90	0.05	4C O to surface along ledge
O-ET			ionized
O-CT	4.90	0.08	6C O to surface near POC
Mg-CT	4.87	0.13	O near POC to surface near POC

[a] For each structure, the coordination of the sites which contribute the most to the initial and final states of the transition are identified. 6C is shorthand for six-coordinated, 5C for five-coordinated, and so on. POC is shorthand for point of contact. [b] Optical properties that depend sensitively on the size of cluster used (see section 4.5).

The features with the lowest excitation energies, covering the range 4.1−4.8 eV, are the low-coordinated corners and step-corners. In the case of the terrace and edge, the relevant electronic states have a delocalized nature; therefore, excitation energies should not be considered quantitatively accurate. In both cases, the final state for the most intense transitions is delocalized along the surface. The terrace excitation spectrum consists of a narrow peak centered at about 5.8 eV, and this compares favorably with the excitation energy of 6.15−6.20 eV extracted from experiments.[51,52] The edge spectrum is much broader, containing three peaks of equal intensity spanning 4.6−5.5 eV; therefore, a single type of excitation cannot be assigned to this range. The multimodal nature of the low-energy excitations at the edge may be consistent with the range of excitation energies of 5.3−5.7 eV that have been reported experimentally.[7,32,53] Qualitatively, one can say that edges are optically excited at much lower energy than terraces (1 eV lower in these calculations); however, the intensity of the edge excitation is weaker.

The strongest excitation for the ledge feature involves a final state which is delocalized along the length of the ledge, and the initial state is localized around the O-terminated end of the ledge. The excitation energy for this type of feature will depend upon the length of the ledge (in this study, the ledge is about 16 Å long and has an excitation energy of 4.9 eV). A distribution of ledge lengths in a real powder may broaden the absorption band from this type of feature.

The metastable and geometrically constrained interfaces (CT and ET) are likely to have a fairly small concentration in reality, with an unknown distribution of local contact angles and strains. Therefore, calculations of the optical properties of particular structures are only indicative. For the ET configuration, ionization would occur (at about 5.9 eV) before significant optical excitation would be observed.

Results for optical excitation of the RC and ET features are not presented because the transitions could not be accurately

(51) Henrich, V. E.; Dresselhaus, G.; Zeiger, H. J. *Phys. Rev. B* **1980**, *22*, 4764−4775.
(52) Cox, P. A.; Williams, A. A. *Surf. Sci. Lett.* **1986**, *175*, L782.
(53) Coluccia, S.; Tench, A.; Segall, R. *J. Chem. Soc., Faraday Trans. 1* **1978**, *74*, 2913.

represented with the quantum clusters. The initial and final states were associated strongly with quantum cluster ions which were adjacent to Mg* ions. However, in the case of the EI feature, the optical excitation would be dominated by the properties of the edges, and the high coordination of the reverse corner features suggests that excitation would not occur below the excitation energy of the terrace.

In summary, these results demonstrate that photons with energies below 5 eV may excite a number of features inside MgO nanopowders. These include not only corners, step-corners, and edges located on the exterior surfaces of the powder[12,27−29] but also ledges which may be found inside the nanopowder as well as on the exterior surfaces.

5. Summary

We have investigated the charge-trapping capabilities of low-coordinated sites at MgO surfaces and interfaces between MgO nanocrystallites and calculated their optical absorption. A wide variety of topological features, which are representative of real nanopowders, have been considered. It seems reasonable, based upon TEM studies and geometrical arguments, that these features should account for the majority of places that may trap electrons or holes.

The calculations of electron affinity reveal that it is unlikely that extra electrons can be trapped at interfaces between nanocrystallites. Among considered structures, only low-coordinated cations on the surface are strong electron traps. One very shallow trap, with an electron affinity of 0.07 eV, was found for the ledge interface. However, such negatively charged ledges would be easily ionized thermally.

The calculation of ionization potentials relative to the vacuum level suggests that delocalized holes may be trapped at a wide variety of interfaces. For these features, there is a barrier for the hole to escape onto terraces and edges due to a difference in ionization potentials of about 0.4 eV. Once on the terrace or edge, the hole is mobile and may become trapped by features such as surface anion corners and step-corners, which are more energetically favorable than interfaces. Holes trapped at these features are strongly localized, and their existence is strongly supported by EPR measurements.[25]

It is well known that modeling localization of extra electrons and holes in different materials is one of the most challenging problems of many-electron theory and that computational methods based on density functional theory often get it wrong (see, for example, ref 54). In addition, both the size of the quantum cluster and the basis set can affect the IPs and the character of the hole localization. The accuracy of the embedded-cluster method and the B3LYP functional for studying these problems in MgO has been demonstrated previously by finding good agreement with experiments for surface ionization and optical excitation energies, properties of localized hole centers, and mechanisms of photo-stimulated desorption.[33] All clusters used in our calculations are treated at a similar level of theory; therefore, we believe that relative comparisons are valid. Systematic improvements to the quality of the calculations can be made by increasing the size of the quantum cluster and improving the basis set. This, however, could not be achieved at the present level of available computer resources.

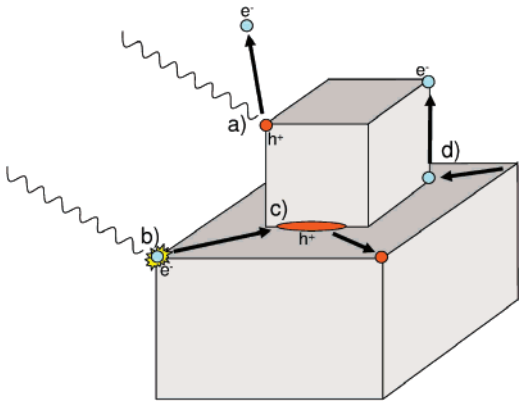

Figure 7. Possible mechanisms of formation of electrons and holes inside the powder and subsequent motion and trapping. See section 5 for more details.

Nevertheless, we believe that the observed hole-trapping at several interfaces between nanoclusters is a genuine effect, which may have important consequences for other oxide materials. The hole confinement at surface features shown in Figures 2−4 is natural and results from the shape and dimensions of the surface features and interfaces considered. The energy difference with the terrace and edge can only increase if holes could be given more variational freedom in more extensive calculations of these surface features.

Photons with energies close to 5 eV are usually used to selectively excite low-coordinated surface sites.[55] Our calculations of optical absorption spectra indicate that a variety of features buried within a powder can be also exited with photon energies less than 5 eV.

Combining these results together with the calculated optical excitations, one can describe a large number of the processes that can happen during and following irradiation of nanopowders. Photons with energy exceeding 7 eV are able to ionize almost any feature at the surface or at interfaces between nanocrystallites, whereas photons with energy around 5−6 eV predominantly ionize low-coordinated surface anions (Figure 7a). Following ionization, the hole can remain trapped where it is formed, or it may migrate to a more favorable position. With photon energies less than 5 eV, excitons can be formed at many interface and surface features. Subsequent absorption of a second photon by the exciton localized at three-coordinated sites, such as Mg-C, O-C, and O-SC, may lead to spatial separation of the electron and hole or to ionization (Figure 7b). Holes that are liberated inside the powder by excitation may become trapped in a delocalized form at an interfaces before escaping to more favorable sites on the exterior of the powder (Figure 7c). Electrons can also be trapped at some interfaces, but in significantly lower concentrations (Figure 7d). We note that studying these processes should now be possible using time-resolved two-photon photoemission spectroscopy,[56] where the effect of temperature on hole escape from interfaces can be investigated.

In conclusion, we find that interfaces between MgO nanocrystallites in a powder are not likely candidates for trapping localized holes as can happen readily at the surface. However,

(54) d'Avezac, M.; Calandra, M.; Mauri, F. *Phys. Rev. B* **2005**, *71*, 205210.
(55) Beck, K. M.; Henyk, M.; Wang, C.; Trevisanutto, P. E.; Sushko, P. V.; Hess, W. P.; Shluger, A. L. *Phys. Rev. B* **2006**, *74*, 045404.
(56) Ge, N.-H.; Wong, C. M.; Lingle, R. L., Jr.; McNeill, J. D.; Gaffney, K. J.;; Harris, C. B. *Science* **1998**, *279*, 202.

delocalized holes may be trapped at interfaces. Trapped, delocalized holes can be freed following annealing sufficient to thermally activate holes onto terraces and edges. On the contrary, there are few places which can trap electrons at interfaces; only the ledge feature was found to have a small positive electron affinity.

Acknowledgment. K.P.M. is supported by the EPSRC (grant GR/S80080/01) and P.V.S. by a Grant-in-Aid for Creative Scientific Research (Grant No. 16GS0205) from the Japanese Ministry of Education, Culture, Sports, Science and Technology. We are grateful to Oliver Diwald and Mario Chiesa for valuable and stimulating discussions and P. E. Trevisanutto for help in calculations and useful comments.

Supporting Information Available: Complete ref 42. This material is available free of charge via the Internet at http://pubs.acs.org.

JA071602M